Journal of Engineering Physics and Thermophysics, Vol. 79, No. 2, 2006

TOPOLOGY OF AN INCOMPRESSIBLE VISCOUS-FLUID FLOW IN A CUBIC CAVITY WITH A MOVING COVER

K. N. Volkov

UDC 532.51

The mechanisms of formation of three-dimensional jet flows inside large-scale vortex structures in a closed cubic cavity have been considered. The vortex structure of an incompressible viscous-fluid flow in this cavity has been investigated using the qualitative theory of ordinary differential equations. Singular points and their types and positions were determined at different Reynolds numbers on the basis of numerical calculations.

Introduction. New methodological conceptions, numerical methods, and computational programs are usually tested using simple-geometry problems with simple boundary conditions. One testing problem of fluid mechanics is the problem on a flow of an incompressible viscous fluid in a cubic cavity with a moving wall. The structure and characteristics of a flow in this cavity were described in detail in the literature [1, 2].

The indicated problem is exactly solved using the biharmonic equation for the vector stream function at Re $\to$ 0 [1]. In other cases, numerical methods are used. There is a large amount of various data that allow one to compare different schemes of solving Navier–Stokes equations and realize the physical sense of a separation flow formed in a cavity. Navier–Stokes equations can be numerically integrated by the control-volume [2], finite-difference [3], and finite-element methods [4].

At Re < 5000, a flow in a cubic cavity is laminar. At Re $\sim$ 2000, the circulation of a fluid in this cavity has a cellular structure with definite inner boundaries between flows [2]. A loss of stability of the flow is preceded by these changes. At Re $\sim$ 3000, a circulation fluid motion in a cubic cavity becomes unsteady and unstable, which manifests itself as an asymmetry of a three-dimensional vortex flow relative to the geometric plane of symmetry [4]. Direct numerical simulation and simulation of large vortices of a flow in a cubic cavity have shown that the change to a turbulent regime happens at Re = 6000–8000 [5, 6], and, at Re = 10^5, the flow becomes completely turbulent [7].

Systematization and analysis of the data obtained made it possible to determine the main structural features of a vortex flow in a cavity and to propose criteria for estimating the quality of the discrete model used [2, 3]. It should be noted that, in this case, the type of singular points of a vortex flow was determined on the basis of visualization of the fluid spreading on the cavity walls. In the present work, the vortex structure of a flow in a cubic cavity was investigated and the singular points were classified with the use of the qualitative theory of ordinary differential equations.

Formulation of the Problem and Numerical Method. Let us consider an unsteady isothermic flow of an incompressible viscous fluid in a cubic cavity with a wall L = 1 m, which is induced by the movement of the upper face with a velocity U = 1 m/sec. The Reynolds number is determined by the length of the cavity side and the velocity of movement of the upper wall: Re = $\rho UL/\mu$. Calculations are performed for a fluid with a density ρ = 1.2 kg/m^3 and a molecular viscosity μ corresponding to a definite Reynolds number. It is assumed that, at the initial instant of time, the fluid is at rest ($u = v = w = 0$, $p = 10^5$ Pa). The boundary conditions of adhesion and nonpercolation are set on the walls of the cavity.

The method used for numerical integration of Navier–Stokes equations is described in [8]. For bunching of grid nodes near the cavity walls, the following transformation of coordinates is used:

$$x_i = \frac{(\beta+1)\left[(\beta+1)/(\beta-1)\right]^{2\bar{x}_i-1} - (\beta-1)}{2\left[1+(\beta+1)/(\beta-1)\right]^{2\bar{x}_i-1}},$$

Voenmekh D. F. Ustinov Baltic State Technical University, 1st Krasnoarmeiskaya Str., St. Petersburg, 190005, Russia; email: dsci@mail.ru. Translated from Inzhenerno-Fizicheskii Zhurnal, Vol. 79, No. 2, pp. 86–91, March–April, 2006. Original article submitted November 9, 2004.

1062-0125/06/7902-0295

where $\beta = (1 - \delta)^{-1/2}$ and $\bar{x}_i = i/n$ for $i = 0, ..., n$. At $\delta \to 0$, grid nodes are bunched near the cavity walls.

Classification of Singular Points of a Flow. Visualization of the surface pattern of vortex fluid flows and analysis of their topological characteristics (positions of critical points and vortices, rate of extension/compression of vortices, rate of drift motion of vortices, maximum vorticity) represent powerful and efficient methods of investigating these flows [9]. It should be noted that the boundaries of three-dimensional separation zones of a flow are related to the initial structure of its singular points [10, 11].

Unlike a three-dimensional flow, the friction stress at a critical point of a two-dimensional flow is equal to zero. In the three-dimensional case, streamlines can come together or come apart from a point (the point of flow attachment or the point of flow separation), unwind or curve into a spiral near a point (focuses), come together or come apart from a line (the line of flow attachment or the line of flow separation). The nodal points represent sinks or skin-friction sources.

In many cases, the so-called limiting streamlines [12] (the lines of viscous-fluid flow on a surface, the tangent to which coincides, at each point of the surface of a body, with the vector of the tangential friction stress at this point) are used for visualization of separation flows. The visualization of the field of a scalar quantity, e.g., the spirality density, is used more rarely [10].

In the three-dimensional case, the streamlines are determined by solving the following system of equations:

$$\frac{dx}{dt} = u\,, \quad \frac{dy}{dt} = v\,, \quad \frac{dw}{dt} = w\,. \tag{1}$$

As a result of solution of this system, we obtain the functions $x(t)$, $y(t)$, and $z(t)$, defining, in the parametric form, a curve (phase trajectory) on the phase plane. A set of phase trajectories corresponding to different initial conditions represents a phase portrait of the system; to construct this portrait, it is necessary to determine the family of integral curves of the equation.

$$\frac{dx}{u\,(x, y, z)} = \frac{dy}{v\,(x, y, z)} = \frac{dz}{w\,(x, y, z)}\,.$$

In accordance with the Cauchy theorem on the existence and uniqueness of the solution of a differential equation, one and only one integral curve passes through each point of the phase plane. The requirements of this theorem break down at the so-called singular points (critical points, at which several or an infinitely large number of integral curves intersect).

Let us consider a small neighborhood of a singular point in the coarse case (a system is called coarse if the whole pattern of trajectories remains unchanged when the right sides of equations and their derivatives are changed insignificantly). The streamlines at each point $\mathbf{r}$ have a vector-field direction $\mathbf{v}(\mathbf{r})$. The differential of the radius-vector $d\mathbf{r}$ along the curve defined by the equation $\mathbf{r} = \mathbf{r}(t)$ is determined by the formula

$$d\mathbf{r} = \frac{d\mathbf{r}\,(t)}{dt}\,dt\,.$$

Let us bring the plane $z_* = 0$ into coincidence with the wall, on which the conditions of nonpercolation and adhesion are set (Fig. 1). The limiting streamlines are determined from the equation

$$\frac{d\mathbf{r}_*}{dt} = \mathbf{v}_*\,(\mathbf{r}_*)\,, \tag{2}$$

where $d\mathbf{r}_*$ determines the local direction of a flow.

For the purpose of investigating the type of singular points, we will consider a linearized system of differential equations defining the motion near the equilibrium position. Linearization of Eq. (2) in the neighborhood of a critical point (at $z_* \to 0$) gives

$$\frac{d\mathbf{r}}{dt} = (A\mathbf{r}_* + \mathbf{b})\,z_*\,.$$

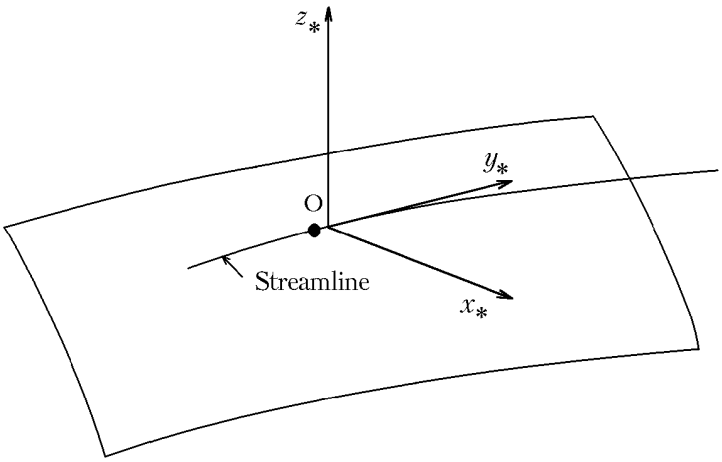

Fig. 1. Determination of the type of singular points.

Since $\mathbf{v}(\mathbf{r}_*) = 0$ at a critical point, $\mathbf{r}_* = -A^{-1}\mathbf{b}$; the flow in the neighborhood of this point is characterized by the eigenvalues and eigenvectors of the Jacobian matrix $A = (\partial\mathbf{v}/\partial\mathbf{r})_*$. The coordinates of singular points and their types are determined by the eigenvalues of the Jacobian determinant.

Let us expand the velocity component in the neighborhood of the point $\mathbf{r}_* = \{x_*, y_*, z_*\}$ by Taylor's theorem. Since the velocity is equal to zero at a critical point,

$$u = \frac{1}{2}\frac{\partial^2 u}{\partial z_*}\bigg|_0 z_*^2 + \ldots + \frac{\partial^2 u}{\partial x_* \partial z_*}\bigg|_0 x_* z_* + \ldots ,$$

$$v = \frac{\partial v}{\partial z_*}\bigg|_0 z_* + \frac{1}{2}\frac{\partial^2 v}{\partial z_*}\bigg|_0 z_*^2 + \ldots + \frac{\partial^2 v}{\partial x_* \partial z_*}\bigg|_0 x_* z_* + \ldots + \frac{\partial^2 v}{\partial y_* \partial z_*}\bigg|_0 y_* z_* + \ldots ,$$

$$w = \frac{\partial w}{\partial z_*}\bigg|_0 z_* + \frac{1}{2}\frac{\partial^2 w}{\partial z_*}\bigg|_0 z_*^2 + \ldots .$$

Neglecting the terms of the order of z_*^2 at $z_* \to 0$, we find

$$\frac{dx_*}{dy_*} = \frac{u}{v} = \frac{\partial^2 u}{\partial x_* \partial z_*}\bigg|_0 x_* \left(\frac{\partial^2 v}{\partial x_* \partial z_*}\bigg|_0 x_* + \frac{\partial^2 v}{\partial y_* \partial z_*}\bigg|_0 y_* \right)^{-1} .$$

The type of a singular point depends on the behavior of the phase trajectories in its neighborhood and is determined by the roots of the characteristic equation $\|A - \lambda U\| = 0$. The following cases are possible:

1) if all the roots are real and negative, there is a stable node, and, if the roots are positive, there is an unstable node;

2) if all the roots are real but different in sign, there arises a saddle, through which only two integral curves (separatrixes) pass;

3) if there is a pair of imaginary conjugate roots, $\lambda_{1,2} = \varphi \pm i\nu$ and $\nu_3 \in R$, there arises a node–focus (if φ and λ_3 have one and the same sign) or a saddle–focus (if φ and λ_3 have different signs).

The formula $\mathbf{r} \to A\mathbf{r}$ at $\|A\| \neq 0$ defines the affine mapping of the space onto itself, which retains its orientation at $\|A\| > 0$ and changes its orientation otherwise. Therefore, if $\|\partial f_i/\partial x_j\| > 0$ ($\|\partial f_i/\partial x_j\| < 0$) at a stationary point, its index is equal to unity (with a negative sign).

Calculation Results. A flow in a cubic cavity was calculated for Reynolds numbers Re = 0–2000 on an 81 × 81 × 81 grid.

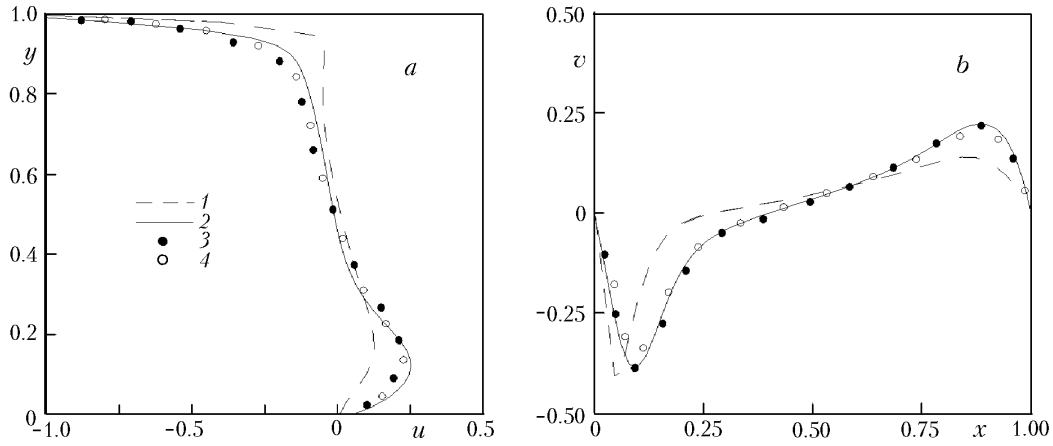

Fig. 2. Distribution of the longitudinal (a) and transverse (b) velocity components in the central cross section of a cubic cavity at Re = 400. Calculations on grids: 1) 31 × 31 × 31; 2) 51 × 51 × 51; 3) 51 × 51 ×51 by the data of [3]; 4) 63 × 63 × 63 by the data of [4].

The data of simulation indicate that the fluid motion in this cavity influences the structure of a vortex flow in it. A decrease in the viscosity of the fluid leads to an intensification of the vortex flow, a displacement of the core of the large-scale vortex to the geometric center of the cavity, and an increase in the sizes of the secondary corner vortices. The maximum values of the velocity components of the reverse flow are lower than those in the two-dimensional variant because of the significant braking effect of the side walls. Moreover, the structure of the primary and secondary vortices in the central cross section of the cavity is spatial in character, which points to the existence of a mass transfer to the central part of the cavity and a mass transfer from its corner regions.

According to the data presented in Fig. 2, the velocity of a three-dimensional flow is lower than the velocity of a two-dimensional flow. When the Reynolds number increases, the difference between the velocity distributions in the central cross section of square and cubic cavities increases. In particular, if this difference is practically absent at Re ~ 100, at Re ~ 400, the maximum difference is 15%, and, at Re ~ 1000, it reaches 22%.

In the patterns of fluid spreading on the walls of the cavity considered, obtained for different Reynolds numbers, we can see singular points of the type of a focus, a center, and a saddle as well as fluid-flow and fluid-spreading lines (Fig. 3a and b). The positions and types of singular points are presented in Fig. 3c and d.

In accordance with the Poincare–Bendixson theorem, there is a relation between the type and number of singular points [12]:

$$\sum N - \sum S = 2 ,$$

where N corresponds to a node or a center and S corresponds to a saddle point. In particular, it follows from Fig. 3c that $\Sigma S = 10$ and $\Sigma N = 12$; consequently, $\Sigma N = \Sigma S + 2$.

At the bottom of a cavity, the development of the fluid spreading with increase in the Reynolds number leads to a decrease in the influence of the side walls and the transformation of a fluid source, at Re = 400, into a spreading line at Re = 1000 (point 11). The indicated source is formed as a result of the attachment of the separation flow in the central region of the cavity to its bottom face. When the Reynolds number increases, point 11 displaces to the geometric center of this face. The separation of the near-bottom flow at the frontal wall of the cavity generates an additional source (point 6) that, as the Reynolds number increases (at Re > 1000), is transformed into a spreading line. Near the edge located upstream of the other cavity elements there arises a saddle point (point 18) and a fluid source (point 21).

Flows outflowing from the indicated sources and propagating over the bottom of the cavity interact along a spreading line. As a result of this interaction, two symmetric peripheral sinks (points 16 and 17) and saddle points

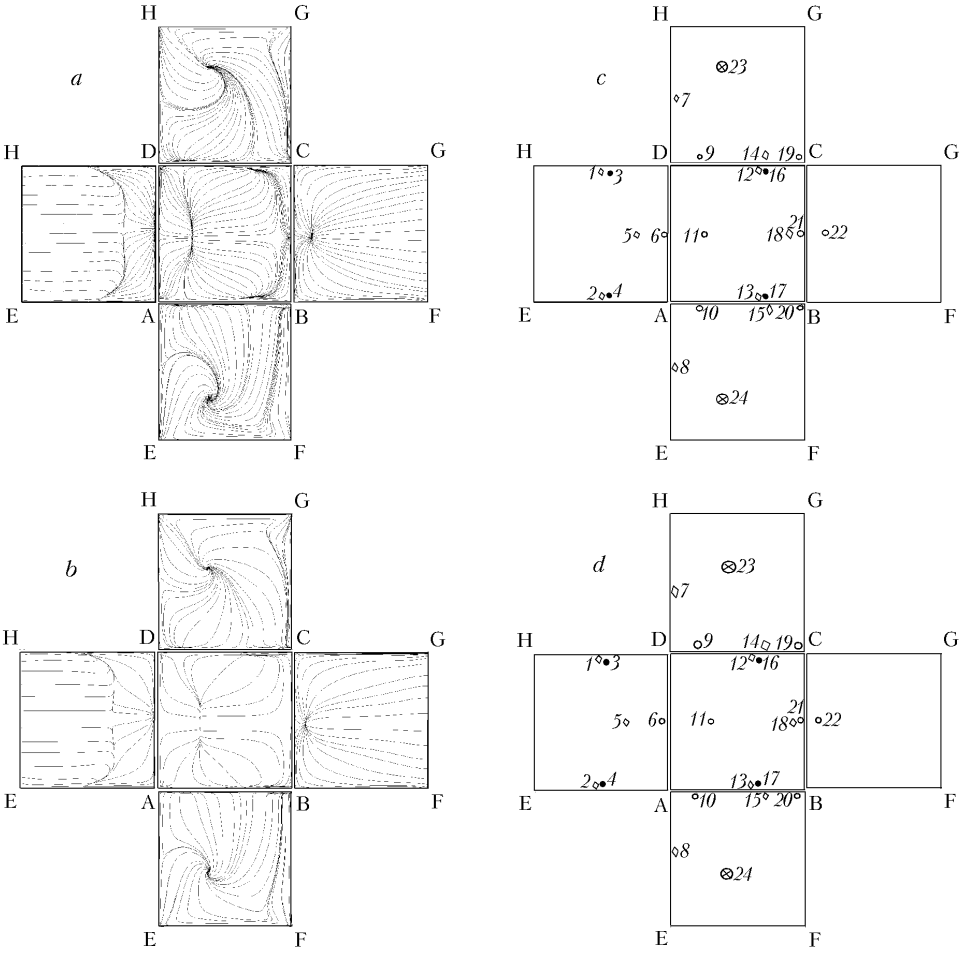

Fig. 3. Patterns of fluid spreading on the walls of the cavity (a, b) and positions of singular points on these walls (c, d) at Re = 400 (a, c) and Re = 1000 (b, d): 1, 2, 5, 7, 8, 12–15, 18) saddle point; 3, 4, 16, 17) stable node; 6, 9–11, 19–22) unstable node; 23, 24) stable focus.

(points 12 and 13) are formed at the bottom of the cavity. When the Reynolds number increases, these points displace upstream to the neighborhood of the edges of the side faces.

At Re = 400, the central zone of a quasi-two-dimensional separation flow is formed at the bottom of the cavity. At Re = 1000, almost half the streamlines covering this region are parallel. When the Reynolds number further increases (Re = 2000), the streamlines covering the central region of the face considered bend.

The fluid flow on the face located upstream of the other cavity elements is determined by the entraining action of the moving wall. When the Reynolds number increases, the flow is transformed — a source (point 6) is transformed into a spreading line. A saddle point (point 5) displaces to the geometric center of the face with increase in the Reynolds number; in this case, points 1–4 displace from the cavity bottom. The liquid motion on the face located downstream of the other cavity elements is caused by the interaction of the shear flow, formed as a result of the movement of the upper cover with a constant velocity, with this wall. Therefore, the majority of streamlines covering the face considered and directed to the bottom of the cavity are practically parallel to its side walls. However, near the bottom of the cavity there arises a source (point 22) induced by the fluid flowing from the bottom of the cavity to its back wall. The interaction of this source with the flow incident from the top down is realized along the spreading line, which with increase in the Reynolds number, becomes parallel to the bottom.

On the side walls of the cavity there arises a swirling fluid motion with a sink (points 23 and 24) outflowing from the central part of the structure. When the Reynolds number increases, this structure displaces to the geometric

center of the side face. On each side face of the cavity, near its bottom, there are also other singular points — two nodes (points 9, 19 and points 10, 20) and one saddle point (points 14 and 15). The positions of these points change insignificantly with increase in the Reynolds number (they displace upstream and approach the bottom of the cavity). Near the edge of each side face, located upstream of the other cavity elements, there arises one more saddle point (points 7 and 8).

Conclusions. Singular points in a vortex flow of a fluid in a cubic cavity and their types and positions have been determined at different Reynolds numbers on the basis of numerical calculations and the qualitative theory of differential equations.

NOTATION

A, Jacobian determinant; **b**, vector; I, unit matrix; L, size of a cavity side, m; n, number of grid nodes; p, pressure, Pa; **r**, radius-vector, m; Re, Reynolds number; t, time, sec; u, v, w, velocity components, m/sec; U, velocity of travel of the upper wall, m/sec; **v**, velocity vector, m/sec; x, y, z, space coordinates; β, δ, coefficients; φ, real part of an eigenvalue; λ, eigenvalue; ν, imaginary part of an eigenvalue; μ, dynamic viscosity, kg/(m·sec); ρ, density, kg/m^3. Subscripts: *, local parameters.

REFERENCES

1. P. N. Shankar and M. D. Deshpande, Fluid mechanics in the driven cavity, *Ann. Rev. Fluid Mech.*, **32**, 93–136 (2000).
2. A. V. Ermishin and S. A. Isaev (Eds.), *Control of Flow past Bodies with Vortex Cells as Applied to Flying Vehicles of Integral Arrangement* (*Numerical and Physical Simulation*) [in Russian], MGU, Moscow–St. Petersburg (2001).
3. T. W. H. Sheu and S. F. Tsai, Flow topology in a steady three-dimensional lid-driven cavity, *Computers Fluids*, **31**, 911–934 (2002).
4. V. Babu and S. A. Korpela, Numerical solution of the incompressible three-dimensional Navier–Stokes equations, *Computers Fluids*, **23**, No. 5, 675–691 (1994).
5. Y. A. Hassan and H. R. Barsamian, New-wall modeling for complex flows using the large eddy simulation technique in curvilinear coordinates, *Int. J. Heat Mass Transfer*, **44**, 4009–4026 (2001).
6. M. D. Deshpande and S. G. Milton, Kolmogorov scales in a driven cavity flow, *Fluid Dyn. Res.*, **22**, 359–381 (1998).
7. J. R. Koseff, R. L. Street, P. M. Gresho, C. D. Upson, and J. A. C. Humphrey, A three-dimensional lid-driven cavity flow: Experiment and simulation, in: J. A. Johnson, C. Taylor, and W. R. Smith (Eds.), *Numerical Methods in Laminar and Turbulent Flow*, Pineridge Press, Swansea, UK (1983), pp. 564–581.
8. K. N. Volkov, Bifurcation of the lines of an incompressible viscous-fluid flow in a rectangular cavity with a moving wall, *Inzh.-Fiz. Zh.*, **79**, No. 2, 81–85 (2006).
9. J. M., Delery, Physics of vorticial flows, *J. Aircraft*, **29**, No. 5, 856–876 (1992).
10. J. L. Helman and L. Hesselink, Visualizing vector field topology in fluid flows, *IEEE Computer Graphics Applications*, **11**, 36–46 (1991).
11. H. Vollmers, Detection of vortices and quantitative evaluation of their main parameters from experimental velocity data, *Meas. Sci. Technol.*, **12**, 1199–1207 (2001).
12. M. J. Lighthill, Attachment and separation in three-dimensional flows, in: L. Rosenhead (Ed.), *Laminar Boundary Layers*, Oxford University Press, Oxford (1963), pp. 72–82.